Gemini Planet Imager coronagraph testbed results

Anand Sivaramakrishnan[a,b], Rémi Soummer[c], Ben R. Oppenheimer[a],
G. Lawrence Carr[d], Jacob L. Mey[a], Doug Brenner[a],
Charles W. Mandeville[a], Neil Zimmerman[a,e], Bruce A. Macintosh[f],
James R. Graham[g], Les Saddlemyer[h], Brian Bauman[f],
Alexis Carlotti[i], Laurent Pueyo[j], Peter G. Tuthill[k],
Christophe Dorrer[l], Robin Roberts[a], Alexandra Greenbaum[m],

[a] American Museum of Natural History, 79th Street at CPW, New York, NY 10024, USA
[b] Stony Brook University, Stony Brook NY 11794, USA
[c] Space Telescope Science Institute, 3700 San Martin Drive, Baltimore, MD 21218 USA
[d] National Synchrotron Light Source, Brookhaven National Laboratory, Upton, NY 11973 USA
[e] Columbia University, 550 West 120th Street, New York, NY 10027 USA
[f] Lawrence Livermore National Laboratory, 7000 East Ave Livermore, CA 94551 USA
[g] Astronomy Department, University of California at Berkeley, CA 94720 USA
[h] Hertzberg Institute of Astrophysics, 5071 West Saanich Road, Victoria BC V9E 2E7 Canada
[i] Princeton University, Princeton NJ 08544 USA
[j] Jet Propulsion Laboratory, 4800 Oak Grove Drive, Pasadena CA 91109 USA
[k] University of Sydney School of Physics 2006 NSW Australia
[l] Aktiwave, 241 Ashley Drive, Rochester, NY 14620 USA
[m] Rensselaer Polytechnic Institute, 110 Eighth Street, Troy, NY 12180 USA

ABSTRACT

The Gemini Planet Imager (GPI) is an extreme AO coronagraphic integral field unit YJHK spectrograph destined for first light on the 8m Gemini South telescope in 2011. GPI fields a 1500 channel AO system feeding an apodized pupil Lyot coronagraph, and a nIR non-common-path slow wavefront sensor. It targets detection and characterizion of relatively young (<2GYr), self luminous planets up to 10 million times as faint as their primary star. We present the coronagraph subsystem's in-lab performance, and describe the studies required to specify and fabricate the coronagraph. Coronagraphic pupil apodization is implemented with metallic half-tone screens on glass, and the focal plane occulters are deep reactive ion etched holes in optically polished silicon mirrors. Our JH testbed achieves H-band contrast below a million at separations above 5 resolution elements, without using an AO system. We present an overview of the coronagraphic masks and our testbed coronagraphic data. We also demonstrate the performance of an astrometric and photometric grid that enables coronagraphic astrometry relative to the primary star in every exposure, a proven technique that has yielded on-sky precision of the order of a milliarsecond.

Keywords: apodized pupil Lyot coronagraph, National Synchrotron Light Source, adaptive optics, coronagraph, coronagraphic astometry, coronagraphic photometry, high-contrast imaging, integral field spectrograph, extrasolar planet

1. INTRODUCTION

Astronomy is at a new frontier of comparative planetary science. Recent advances in adaptive optics (or AO, which corrects atmospheric disturbances to stellar light in real-time), combined with coronagraphy, a technique for suppressing the diffracted flood of light from a star to search its environs for planetary companions and faint protoplanetary disks, will enable the direct detection of warm young extrasolar Jupter-like planets within 50

Further author information: (Send correspondence to A.S.) A.S.: E-mail: anand@amnh.org, Tel: 1 212 313 7653

Ground-based and Airborne Instrumentation for Astronomy III, edited by Ian S. McLean,
Suzanne K. Ramsay, Hideki Takami, Proc. of SPIE Vol. 7735, 773586 · © 2010
SPIE · CCC code: 0277-786X/10/$18 · doi: 10.1117/12.858623

parsecs of our Sun. These planets are at least 7 orders of magnitude fainter than their parent stars in the H and K spectral bandpasses (with central wavelengths of 1.65 and 2.1 microns respectively).

The Gemini Planet Imager (GPI) is a near-IR 'extreme AO' (ExAO) coronagraphic instrument being developed for the twin 8 m Gemini telescopes. With an advanced AO system operating at 2kHz, and 1500 channels of wavefront sensing and correction over an 8 m primary mirror, it is designed to provide a sufficiently flat stellar wavefront to a coronagraph to enable the requisite coronagraphic suppression demanded by these science goals.

2. INSTRUMENT OVERVIEW

GPI consists of six integrated subsystems.

1. *The opto-mechanical superstructure (OMSS) led by HIA* mounts and connects all the subsystems and mates to the Gemini ISS. The AO optics and elements mount directly to the OMSS optics bench, while a flexure-sensitive frame holds other major subsystems.

2. *The adaptive optics system (AO) led by LLNL*, responsible for fast measurement of the instantaneous wave front, and for providing wave front control via deformable mirrors. The optical components and mechanisms for the AO system are provided by the OMSS.

3. *The calibration unit (CAL) led by JPL* is a high-accuracy infrared wave front sensor tightly integrated with the coronagraph. The CAL high-order wavefront sensor (HOWFS) is an interferometer that provides precise and accurate measurements of the time-averaged wave front at the science wavelength and coronagraph focal plane, so that persistent speckles caused by quasi-static wave front errors do not dominate the final image. The CAL low-order wavefront sensor (LOWFS) is a small Shack-Hartmann sensor that provides pointing, focus, and low-order aberration sensing to keep the target star centered on the coronagraph. It provides GPI with a unique capability to achieve and sustain systematic wavefront errors at the nanometer level.

4. *The coronagraph subsystem (COR) led by AMNH* uses a combination of apodized masks and focal plane stops to control diffraction and pinned speckles.

5. *The science instrument (IFS) led by UCLA and University of Montreal*, is an integral field spectrograph that produces the final scientific image or data cube, including simultaneous multiple wavelength channels to suppress residual speckle noise, and a dual-channel polarimetric capability. It also provides a diagnostic pupil-viewing mode and contains the final Lyot stop for the coronagraph.

6. *The Top-Level Computer (TLC) produced by HIA*, coordinates sequencing and communication between subsystems, and between GPI and the observatory. It also provides motion control for all the subsystems.

3. GPI CORONAGRAPH

The baseline coronagraph for GPI is the Apodized Pupil Lyot Coronagraph (APLC).[4] The light from the AO system is passed through a pupil plane A containing a transmissive apodizer mask that tapers the intensity of light across the pupil. The light is brought to a focus at a focal plane mask (FPM) where the central core of the PSF is removed. The off-axis light continues to the re-imaged pupil. The combination of the initial apodizer and the focal plane mask channels the coherent portion of the on-axis light outside the re-imaged pupil, where it is blocked by a Lyot stop. In the final focal plane, at the design wavelength, diffraction is almost perfectly suppressed. In the GPI architecture, as in the Lyot Project and P1640 coronagraphs, the FPM is a super polished mirror with a central hole, allowing the on-axis light to pass into the CAL system. The final Lyot stop is located inside the IFS dewar.

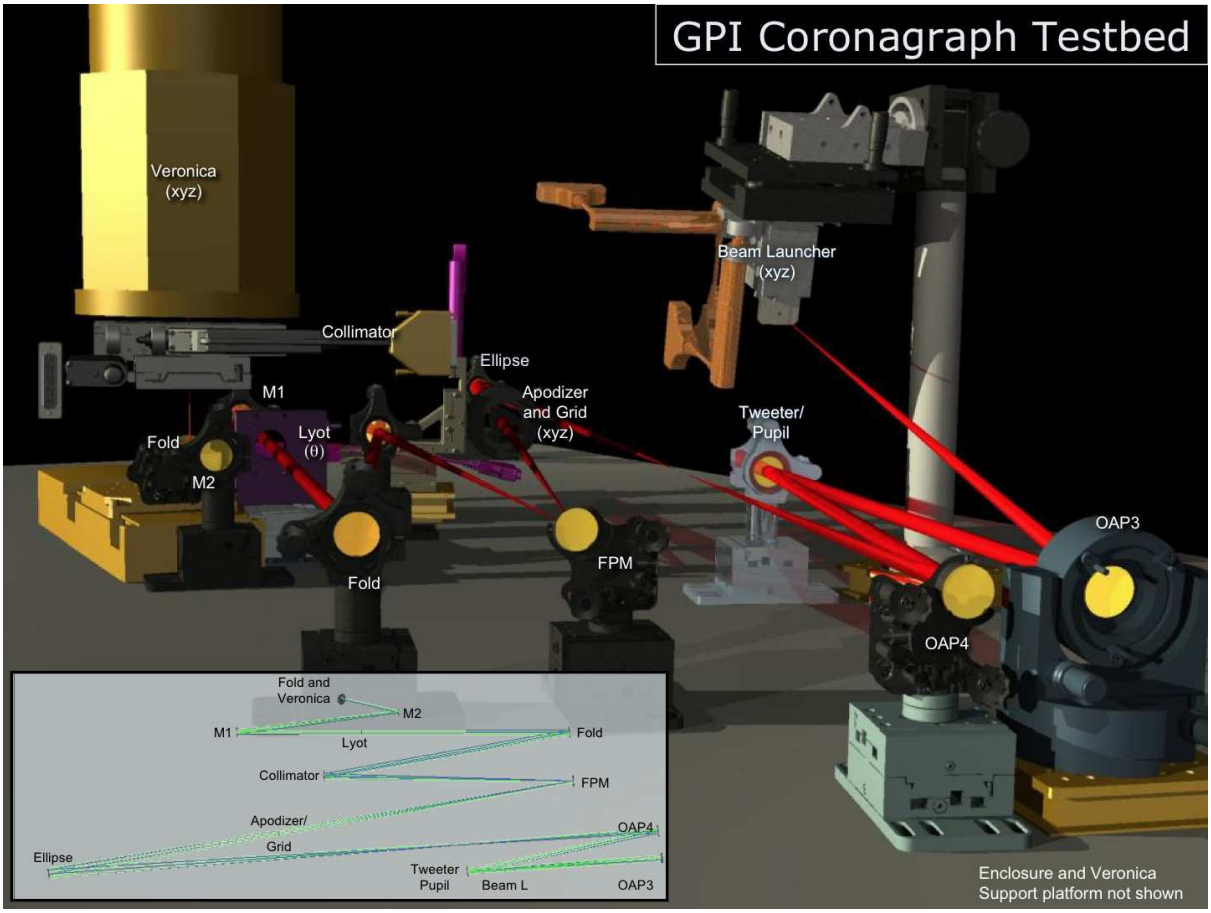

Figure 1. A solid model showing the AMNH coronagraphic testbed, with the optical train in the inset.

4. THE AMNH NEAR-IR CORONAGRAPHIC TESTBED

The near IR JH testbed at AMNH provided a proving ground for the technology required to develop GPI's coronagraphic masks. The testbed consists of a passive, all-reflective optical train that is very similar to the GPI post-AO system optical train.

The testbed is fed with a supercontinuum IR laser. A mirror with a stop on its surface is illuminated with a collimated beam on the testbed. This forms the testbed's input pupil. This pupil is reimaged to a pupil image where a first coronagraphic mask is placed. This is an apodizer. A subsequent focal plane is created, again, with the same $f/64$ beam that GPI will use, on a superpolished mirror with a clean-edged hole at its center. This is the focal plane mask (FPM). The light reflected by the FPM then strikes another powered mirror to create a Lyot plane with the GPI size and geometry. After passing through a Lyot stop in this plane, the beam is focussed on to Veronica, a NICMOS camera which records J and H data. This camera is modeled after MONICA,[1] although all optics after the dewar window were removed for use on the testbed. The camera is not equipped with a Y filter, and the lack of a cold stop made K band imaging impractical for thermal reasons. The testbed's wavefront error is of the order of 30nm.[19]

5. CORONAGRAPH DESIGN

Although the apodized pupil Lyot coronagraph (APLC)[2–5] is a robust high-throughput coronagraph suitable for detecting young Jovian planets around nearby stars, it is, like most Lyot coronagraphs, inherently chromatic. It operates by carefully matching the pupil plane response of its FPM to the apodizer mask. Since the FPMs

effective size in units of λ/D is obviously a function of wavelength. By optimizing the Lyot stop geometry the APLC apodizer/FPM combination was optimized a specific 20% bandpass at Y, J, H and two bandpasses covering K. The chosen APLC mask set has excellent achromatic performance, but somewhat limited contrast in the region of 3-5λ/D.

5.1 Apodizer design

The apodizer design utilizes a grey (i.e. non-chromatic) apodizer technology refined specifically for the GPI application. With an approximately 12mm pupil diameter at the apodizer, we used an aluminum-on-chromium 10 micron square metallic dot pattern. The possible dot locations are on a 10 micron grid. This size was determined after extensive testing of test patches with 2, 5, and 10 micron metallic dots on a glass substrate. The apodizer is anti-reflection (AR) coated for IR wavelengths, to improve coronagraphic throughput as well as to minimize back-reflections and ghosting. On the AMNH testbed as well as the actual GPI instrument the pupil image where the apodizer is located is formed in an $f/64$ converging beam. This results in about 1-2mm acceptable placement error of the apodizer along the beam.

5.1.1 Spider effects

As previous work[5] has shown, the APLC design is more tolerant of spider support obstructions in the telescope pupil than the higher contrast Band-Limited coronagraph[6] design. Three of the four Gemini secondary support spiders are 10mm wide, the fourth being 14mm thick. With an effective clear diameter of 7.7701m on Gemini South, these spiders, when appropriately masked in the Lyot plane, do not degrade coronagraphic contrast enough to limit GPI's intended science.

5.1.2 Focal plane stop effects in the Lyot plane

The focal plane contains a field stop that restricts the field of view (FOV). Restricting the FOV at first focus to 120 resolution elements (at 1.65 micron) suggests that oversizing of spider vanes in the Lyot plane mask needs to be about 1% due to ringing induced by the finite FOV.

Thus spider vane oversizing accounts for 1% OD for pupil placement, 1% Lyot stop placement, 0.5 degree rotational tolerance (which translates to about 0.5% OD), and an additional 1% due to Lyot plane ringing from the field stop. A conservative tolerance of 4% of pupil OD is the baseline. If Fresnel-type ringing is expected in the Lyot pupil this oversizing might need to be increased. A range of Lyot stops were made to enable a range of spider oversizing choices to be made. On the AMNH testbed the spider vane is 700 microns wide (on a 10mm pupil) provided best suppression of spiders. However, considering that the astigmatism inherent in the testbed design (as opposed to the GPI instrument itself) broadens features of the pupil image at the Lyot plane, it is likely that GPI will typically use a Lyot stop with thinner spider vane obstructions. This astigmatism[19] (about 25-30 nm) is likely the largest wavefront error before the FPM on the testbed.

5.1.3 Apodizer fabrication

Half-tone screens have been studied for the ESO-SPHERE and other projects in some detail.[7–9] However, the GPI coronagraphic instrument requires a factor of ten or so more light suppression than the comparable ESO-SPHERE coronagraph,[10] as their search spaces and detection methods are slightly different.[11] We refined the methods of writing controlled greyscales on Suprasil glass to achieve our required apodizer profile with sufficient accuracy. With the cooperation of the apodizer vendors Aktiwave (Rochester, NY) and Precision Optical Imaging (Rush, NY) we developed sophisticated calibration and writing methods. Here we summarize the detailed description of apodizer fabrication methods developed for GPI. These were presented in full in earlier work.[12]

We measured the optical density of calibration test patches with transmissions as low as 1% (*i.e.*, an on-axis intensity attenuation factor of 0.01). GPI's pupil masks' apodization profiles need to match the design profile to about ∼0.5% or better. We found continuous opacity material too chromatic for our purposes. We rediscovered anomalously high transmission of light through wavelength-sized holes in metallic screens (*e.g.,* Refs. 13,14 and references therein). Increasing the half-tone screen's dot size to 10 μm on a side enable grey apodizers to be fabricated with the requisite accuracy. Test patches with 5 and especially 2 μm dots exhibited rather complex behaviors, particularly when the microdot screens were laid down in periodic patterns such as a checkerboard, as can occur for a desired 0.5 on-axis far-field transmission.

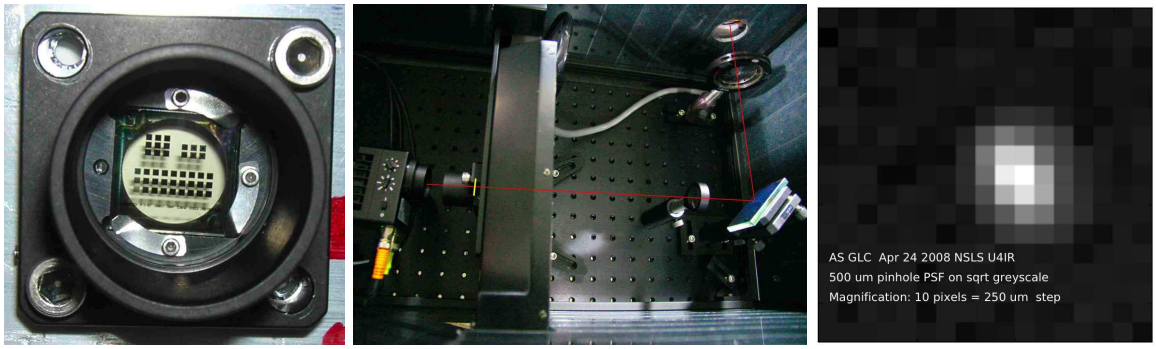

Figure 2. *Left:* Example of a set of calibration patches on a sample, which is mounted in a lens tube. *Middle:* Experimental arrangement. The collimated IR synchrotron beam enters a Bruker 66V Fourier Transform Spectrometer, with its output beam passing through a the circular hole cut in an enclosure. The beam (red line) then passes through an iris diaphragm used to set the desired focal ratio. After reflecting off a fold mirror it is focussed by an IR doublet on the sample mounted on a computer-controlled stage. The sample location is indicated with a small yellow bar drawn transverse to the beam. This stage is the only optomechanical part of the set-up moved during the measurement of a sample. The single-channel InGaAs detector at left in this panel is about 2 mm square. The detector output goes to the FTIR spectrometer. *Right:* PSF of beam on sample measured through a low-quality 500um pinhole at focus (instead of the sample). The spatial step size in this grid is 250 μm. This and other PSF measurements suggest a PSF size of about 200 μm in one direction and 100 μm in the other.

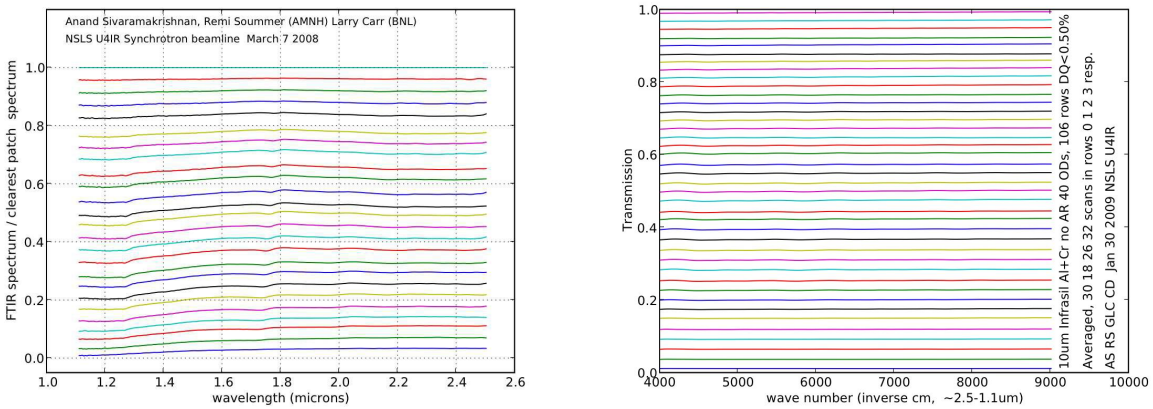

Figure 3. *Left:* Spectra of uniform optical density (OD) calibration patches fabricated with 2 μm metallic microdots. Chromaticity is far less than for the continuous opacity material, but is still visible from the fact that the curves are not horizontal. The substrate, infrasil, shows hydroxyl features that complicate the transmission. *Right:* Spectra of uniform optical density (OD) calibration patches fabricated with 10 μm metallic microdots. The substrate, Suprasil 301, does not show strong hydroxyl absorption.

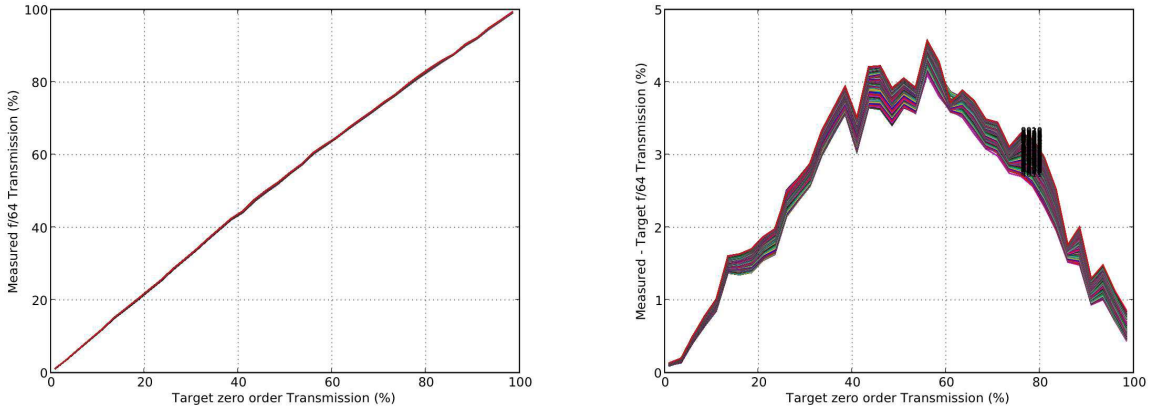

Figure 4. 10 μm microdot patch transmission accuracy for all 40 OD patches: *Left:* target vs. measured *Right*: target vs. measured minus target. This transmission error was fed back into the microdot placement algorithm for the final apodizer manufacture.

5.1.4 Apodizer wavefront error

The wavefront error in the glass apodizers was measured at 1.55 microns at Zygo Corporation (Middlefield, CT), in a double-pass configuration. We present a sample wavefront measurement here. The OPD across the apodizer is typically well-behaved, although there are occasional excursions near the edges of the apodizer, where the optical density climbs.

5.1.5 Apodizer technology calibration using IR synchrotron radiation

The UV-Optical electron ring at the National Synchrotron Light Source (NSLS) at Brookhaven National Laboratory (BNL) provides a photometrically and optically stable well-collimated IR light source with a compact point-spread function (PSF). It is powerful enough for accurate measurements, in addition to being understood optically. Experimental paradigms used at the U4IR beamline at NSLS are well-defined, enabling beam intensity fluctuations to be calibrated out to well below our desired transmission measurement accuracy.

The U4IR beamline at the NSLS extracts synchrotron radiation from an 800 MeV electron storage ring. The electrons emit the synchrotron radiation as they are tangentially accelerated through one of the dipole magnets used to keep the electrons on an approximately circular orbit. As a "white" source, the spectral range extends from the far-infrared up through the visible and into the soft X-ray spectral region. The beam of electrons is reasonably small (a few hundred microns across) and the highly relativistic aspect of the electrons causes the radiated light to be emitted into angles of a few milliradians. This combination of small source size and narrow angular emission results in a high source brightness, in some cases 2 to 3 orders of magnitude brighter than conventional thermal sources. High brightness is important when the optical system being employed has a reduced throughput. In our case, the low throughput is a necessary condition of the large focal ratio ($f/64$) required to mimic the diffractive conditions that hold for both the AMNH testbed as well as the GPI instrument.

For our measurement, the visible and near-infrared part of the synchrotron radiation spectrum is collected and spectroscopically analyzed using a Bruker 66v Fourier transform infrared spectrometer (FTIRS) equipped with a CaF_2 beamsplitter and InGaAs photodiode detector. The detector's wavelength range was 1.1 - 2.5 μm. We used a spectral resolution of 100 across the range. Our sample was mounted on a computer-controlled X-Y stage with sub-micron positional repeatability. The experiment was run using a proprietary Bruker stage and FTIRS control macro language (OPUS). Spectral data were translated to ascii files recording wavenumber and throughput at each wavenumber.

A 3mm iris in front of a 200mm focal length doublet lens selected part of the synchrotron beam (whose cross section is of the order of a few centimeters). The beam position is set by means of fold mirrors with manually adjustable tilts. The beam passing through the iris was focussed to a spot of the order of 200 μm in size (Fig. 2).

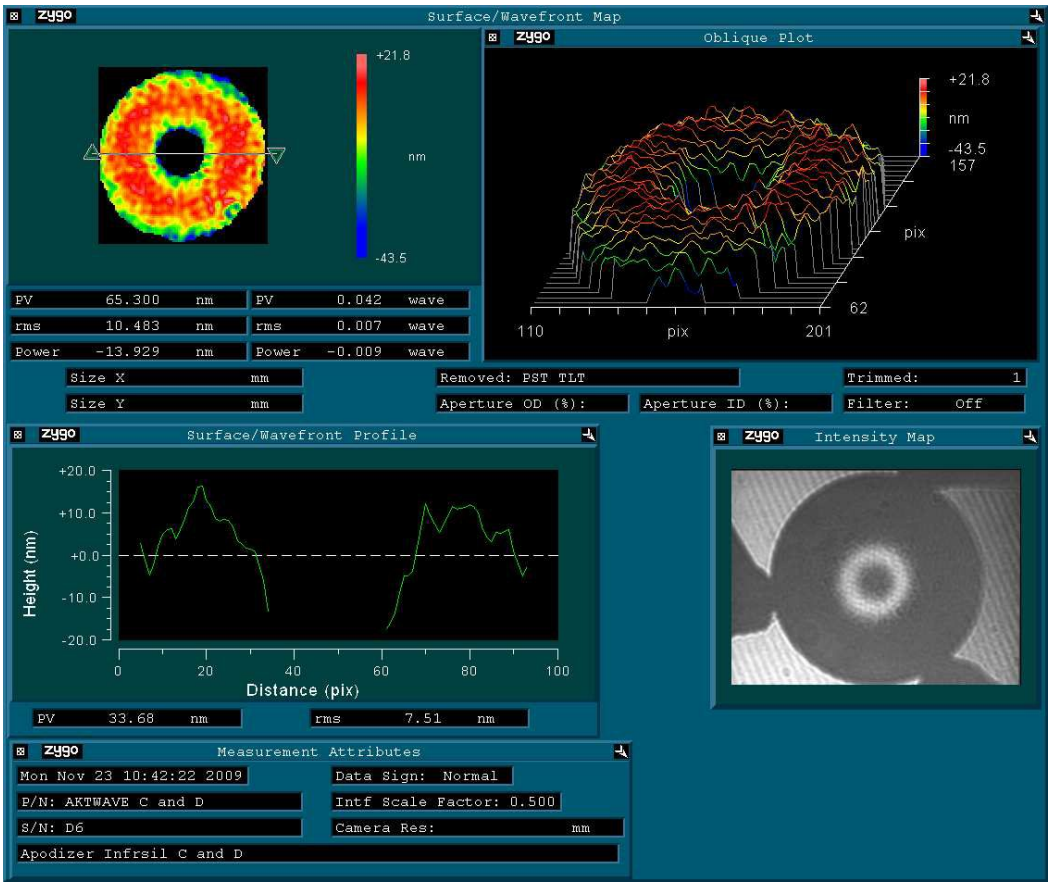

Figure 5. A typical apodizer wavefront error (optical path delay measured in a double-pass transmission configuration), measured at 1.55 micron wavelength. This is an H-band apodizer fabricated with 10 micron aluminum-on-chromium microdots.

The internal scatter of measurements stayed below $\sim 0.2\%$. A tradeoff between beam stability and the signal to noise ratio in each spectral scan was explored to find suitable combinations.

5.1.6 Focal plane masks

The focal plane masks (Fig. 6) are implemented as clean holes in superpolished 23.23mm disks ($<$ 3 angstrom roughness over clear aperture). The RMS surface with piston and tilt removed is of the order of 12 nm for three of the four FPMs, and 4nm for the fourth. Roundness of each of the four FPM holes, in the 380-750 micron diameter range, is within 2 microns. There are few defects on the hole edges, as revealed by confocal microscopy at AMNH. These components were cored from selected areas of superpolished silicon wafers, and the through holes that serve as coronagraphic occulters created by a Deep Reactive Ion Etching (DRIE) process. They were manufactured by Jenoptik Optical Systems Inc, Hunstville AL. Our experince with these components indicated that they were as difficult to fabricate as the apodizers themselves.

5.2 Lyot stops

The Lyot stops for GPI were the easiest coronagraphic components to manufacture (Fig 7. They were created using carbon electrode discharge machining by CTM Corporation, Frankfort, NY. Epner Technology, Brooklyn, NY coated the two surfaces with their trademark Laser Black metallic dendrites. This matte surface does not chip or flake when vibrated ultrasonically in acetone, and is space-qualified. It is unlikely that these surfaces would need recoating, although Laser Black's $\sim$ 10 micron sized dendrites cannot be touched without damage. The Lyot stops are cryogenic in GPI, so were manufactured to be the designed size at LN2 temperatures. The

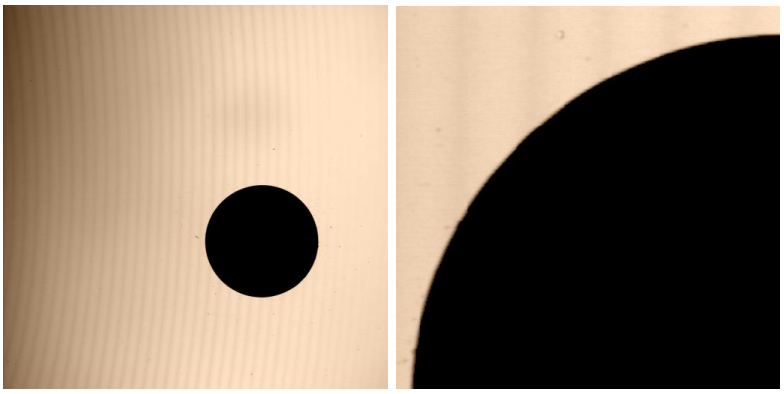

Figure 6. Confocal microscopic image of a GPI focal plane mask. The striations visible in the image are the result of the scans of the confocal visible light microscope over the specimen. They do not imply variations in reflectance. These images are taken to examine the hole quality in the mask. *Left:* 383 micron diameter Deep Reactive Ion Etched hole in the gold-coated silicon mirror that serves as the Y-band focal plane mask for GPI. *Right:* A closeup showing hole ege quality. The holes were round to approximately 1 to 1.5 microns.

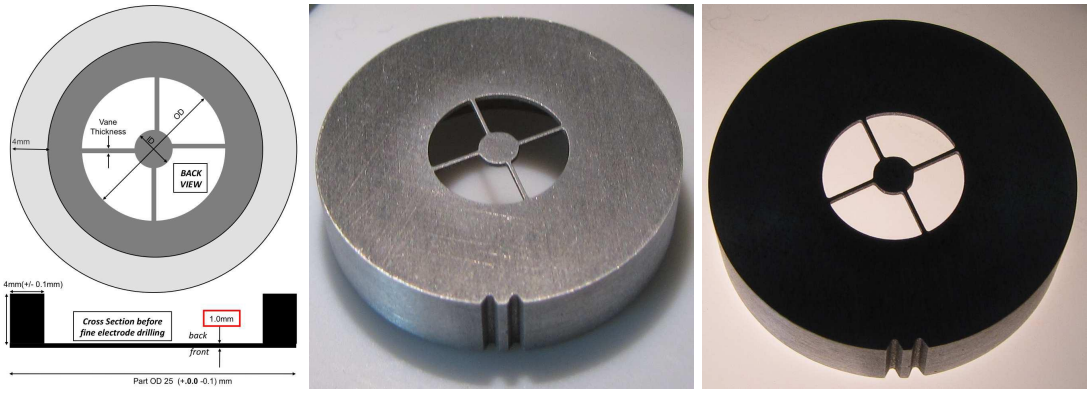

Figure 7. An aluminum carbon electrode drilled Lyot stop. *Left:* A sketch of the basic design. *Middle:* A manufactured Lyot stop prior to coating with the proprietary Epner Laser Black coating. *Right:* A coated part. Both faces are coated. The 'cupped' face faces the incoming beam. The Lyot stops will reside in the dewar of the IFS.

only point of note in their fabrication is that they had to be made thick enough transverse to the beam, so the spider vane obstructions are mechanicaly strong enough to withstand vibrations and the Laser Black process.

6. ASTROMETRY AND PHOTOMETRY

In order to perform astrometry and photometry on coronagraphic images that cannot image the bright primary star along with faint nearby structure or companions in the same exposure, schemes of creating satellite spots by placing a fine grid over a pupil plane have been devised and tested on laboratory testbeds.[15,16] Such a grid provided milliarcsecond photometry on coronagraphic IFU images on P1640 on Palomar Hale a near-IR coronagraphic IFU with a similar configuration to GPI.[17] Fig. 8 shows such spots, and the pupil-plane grid written directly on the apodizer.

For GPI our desired satellite spot brightnesses are of the order of 10 astronomical magnitudes fainter than the central star's image in the absence of an occulting coronagraphic focal plane mask. Simple Fraunhofer theory was used to select a grid thickness. We measured the grid-generated satellite spots in the J and H bands, the satellite spot magnitudes are in approximate agreement with theory.

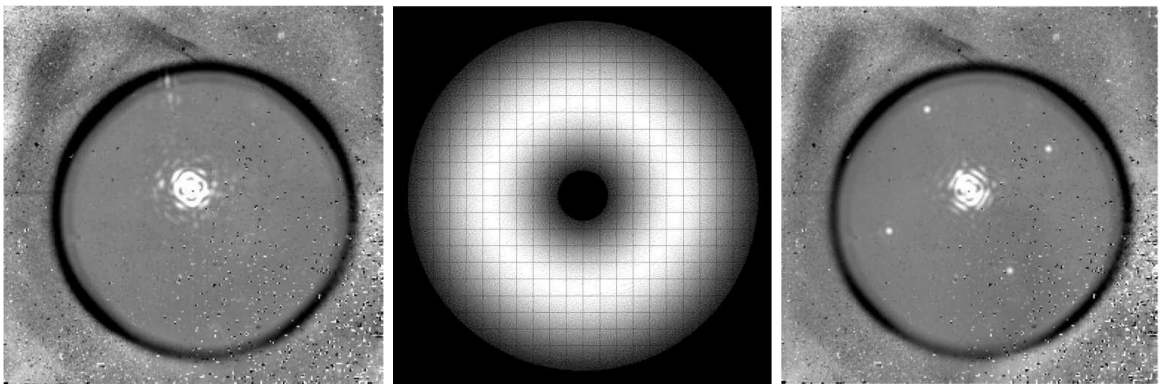

Figure 8. *Left:* A 1.65 μm coronagraphic image used without an astrometric grid in the pupil. *Middle:* Microdot apodizer with an example of a fine opaque grid. *Right:* A 1.65 μm coronagraphic image showing the coronagraphic PSF and the first set of four satellite spots generated by such a grid in the pupil.

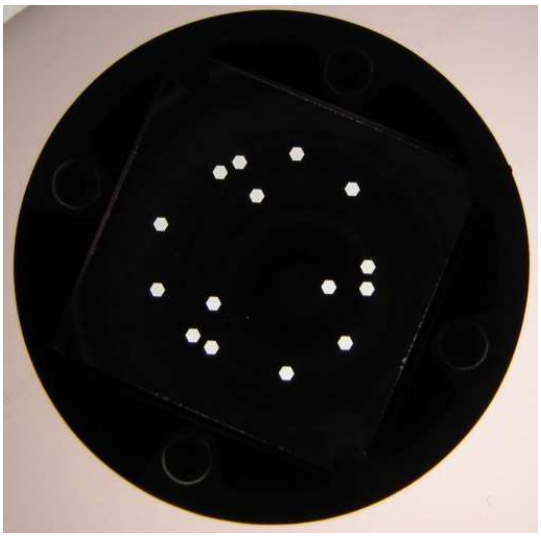

Figure 9. The non-redundant aperture mask with 15 625-micron flat-to-flat hexagonal holes in the 12mm reimaged pupil.

Table 1. Astrometric and photometric fiducial satellite image brightness (magnitudes)

Wavelength (μm)	Contrast (mag)
1.200	9.4
1.250	9.1
1.300	9.4
1.350	9.1
1.550	9.7
1.650	9.6
1.725	9.6
1.799	9.6

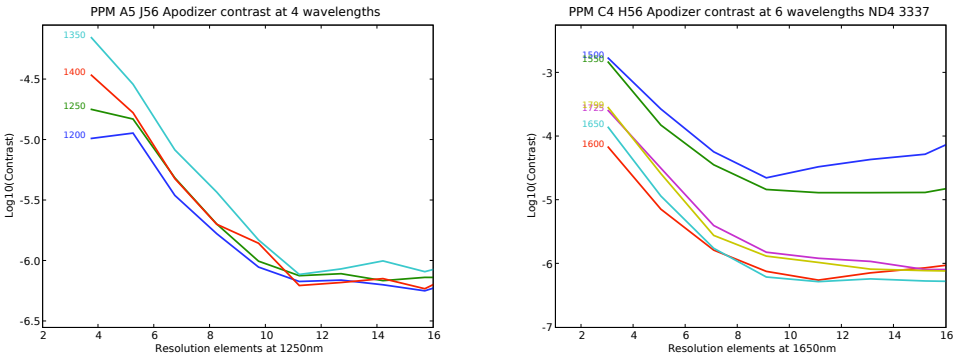

Figure 10. *Left:* Contrast at four wavelengths (labelled in nm)) in J with the $5.6\lambda/D$ stop at band center. *Right:* Contrast at six wavelengths in H with the $5.6\lambda/D$ stop at band center. The contrast at 1500 and 1550 nm is markedy poorer than that at 1600, 1650, 1725, and 1799 nm.

7. NON-REDUNDANT MASK ON GPI

In deciding between aggressive optimization of a coronagraph that achieves an inner working angle of about $4\lambda/D$ and other approaches, we explored the idea of more stringent apodizer designs. However the concept of a non-redundant mask[18] appeared to be a significant risk mitigator, in addition to providing angular resolution that would otherwise be beyond the reach of GPI. A 15-hole mask (Fig. 9) was designed, bringing a wider search space and better Fourier coverage than a higher throughput mask with fewer and larger holes. The inner working angle of the mask is of the order of $\lambda/2D$.

8. IN-LAB PERFORMANCE

The in-lab performance has been described in some detail in an earlier paper.[19] We present the final apodizer contrast curves (Fig. 10), which are consistent with the cited work, including the modeling described therein. The masks that create these contrast curves will be integrated into the full GPI instrument, and we will report on their performance with the improved optical quality enabled by GPI's AO system during interration and testing, before GPI goes on-sky in 2011.

9. CONCLUSION

The AMNH testbed demonstrates, through a combination of design, simulation, lab data, and optical modelling that the broad band apodized pupil Lyot coronagraph in the Gemini Planet Imager will deliver sufficient raw

contrast between its inner working angle and the adaptive optics control radius for the instrument to plausibly meet its primary science goals. A combination of other noise reduction techniques, namely active control of slowly-varying speckles to the nanometer level, and angular differential imaging, will reduce residual speckle noise in the coronagraphic image significantly, to enable direct detection and characterization of warm jovians around nearby stars. The prime spectral bandpass for such efforts is the H band, particularly in discriminating between simultaneous on-band and off-band images in GPI's hyperspectral data cubes. A range of other science, including that enabled by the small inner working angle of non-redundant masking, and simultaneous dual polarization coronagraphic broad band imaging of disks around nearby stars, will also be enabled by the coronagraph.

ACKNOWLEDGMENTS

We acknowledge useful discussions with Daren Dillon (UCSC), John Filhaber (Zygo Corporation), Christian Marois (HIA), and Tom Weinacht (Stony Brook). This work has been partially supported by the National Science Foundation Science and Technology Center for Adaptive Optics, managed by the University of California at Santa Cruz under cooperative agreement AST-9876783, National Science Foundation grant AST-0804417, and NASA award APRA08-0117.

REFERENCES

[1] R. Doyon, D. Nadeau, M. Riopel, A. F. J. Moffat, S. Demers, P. Bastien, and H. Yee, "The Montreal Infrared Camera (MONICA).," *JRASC* **85**, pp. 182–+, Aug. 1991.

[2] C. Aime, R. Soummer, and A. Ferrari, "Total coronagraphic extinction of rectangular apertures using linear prolate apodizations," *A&A* **389**, pp. 334–344, 2002.

[3] R. Soummer, C. Aime, and P. E. Falloon, "Stellar coronagraphy with prolate apodized circular apertures," *A&A* **397**, pp. 1161–1172, Jan. 2003.

[4] R. Soummer, "Apodized Pupil Lyot Coronagraphs for Arbitrary Telescope Apertures," *ApJ* **618**, pp. L161–L164, Jan. 2005.

[5] A. Sivaramakrishnan and J. P. Lloyd, "Spiders in Lyot Coronagraphs," *ApJ* **633**, pp. 528–533, Nov. 2005.

[6] M. J. Kuchner and W. A. Traub, "A Coronagraph with a Band-limited Mask for Finding Terrestrial Planets," *ApJ* **570**, pp. 900–908, May 2002.

[7] C. Dorrer and J. D. Zuegel, "Design and analysis of binary beam shapers using error diffusion," *Journal of the Optical Society of America B Optical Physics* **24**, pp. 1268–1275, June 2007.

[8] P. Martinez, C. Dorrer, E. Aller Carpentier, M. Kasper, A. Boccaletti, K. Dohlen, and N. Yaitskova, "Design, analysis, and testing of a microdot apodizer for the Apodized Pupil Lyot Coronagraph," *A&A* **495**, pp. 363–370, Feb. 2009.

[9] P. Martinez, C. Dorrer, M. Kasper, A. Boccaletti, and K. Dohlen, "Design, analysis, and testing of a microdot apodizer for the apodized pupil Lyot coronagraph. II. Impact of the dot size," *A&A* **500**, pp. 1281–1285, June 2009.

[10] J.-L. Beuzit, M. Feldt, K. Dohlen, D. Mouillet, P. Puget, F. Wildi, L. Abe, J. Antichi, A. Baruffolo, P. Baudoz, A. Boccaletti, M. Carbillet, J. Charton, R. Claudi, M. Downing, C. Fabron, P. Feautrier, E. Fedrigo, T. Fusco, J.-L. Gach, R. Gratton, T. Henning, N. Hubin, F. Joos, M. Kasper, M. Langlois, R. Lenzen, C. Moutou, A. Pavlov, C. Petit, J. Pragt, P. Rabou, F. Rigal, R. Roelfsema, G. Rousset, M. Saisse, H.-M. Schmid, E. Stadler, C. Thalmann, M. Turatto, S. Udry, F. Vakili, and R. Waters, "SPHERE: a planet finder instrument for the VLT," in *Society of Photo-Optical Instrumentation Engineers (SPIE) Conference Series*, *Society of Photo-Optical Instrumentation Engineers (SPIE) Conference Series* **7014**, Aug. 2008.

[11] B. A. Macintosh, J. R. Graham, D. W. Palmer, R. Doyon, J. Dunn, D. T. Gavel, J. Larkin, B. Oppenheimer, L. Saddlemyer, A. Sivaramakrishnan, J. K. Wallace, B. Bauman, D. A. Erickson, C. Marois, L. A. Poyneer, and R. Soummer, "The Gemini Planet Imager: from science to design to construction," in *Society of Photo-Optical Instrumentation Engineers (SPIE) Conference Series*, *Society of Photo-Optical Instrumentation Engineers (SPIE) Conference Series* **7015**, July 2008.

[12] A. Sivaramakrishnan, R. Soummer, G. L. Carr, C. Dorrer, A. Bolognesi, N. Zimmerman, B. R. Oppenheimer, R. Roberts, and A. Greenbaum, "Calibrating IR optical densities for the Gemini Planet Imager extreme adaptive optics coronagraph apodizers," in *Society of Photo-Optical Instrumentation Engineers (SPIE) Conference Series*, *Society of Photo-Optical Instrumentation Engineers (SPIE) Conference Series* **7440**, Aug. 2009.

[13] T. W. Ebbesen, H. J. Lezec, H. F. Ghaemi, T. Thio, and P. A. Wolff, "Extraordinary optical transmission through sub-wavelength hole arrays," *Nature* **391**, pp. 667–669, Feb. 1998.

[14] C. Genet and T. W. Ebbesen, "Light in tiny holes," *Nature* **445**, pp. 39–46, 2007.

[15] A. Sivaramakrishnan and B. R. Oppenheimer, "Astrometry and Photometry with Coronagraphs," *ApJ* **647**, pp. 620–629, Aug. 2006.

[16] C. Marois, D. Lafrenière, B. Macintosh, and R. Doyon, "Accurate Astrometry and Photometry of Saturated and Coronagraphic Point Spread Functions," *ApJ* **647**, pp. 612–619, Aug. 2006.

[17] N. Zimmerman, B. R. Oppenheimer, S. Hinkley, D. Brenner, I. R. Parry, A. Sivaramakrishnan, L. Hillenbrand, C. Beichman, J. R. Crepp, G. Vasisht, L. C. Roberts, R. Burruss, D. L. King, R. Soummer, R. Dekany, M. Shao, A. Bouchez, J. E. Roberts, and S. Hunt, "Parallactic Motion for Companion Discovery: An M-Dwarf Orbiting Alcor," *ApJ* **709**, pp. 733–740, Feb. 2010.

[18] P. G. Tuthill, J. D. Monnier, and W. C. Danchi, "A dusty pinwheel nebula around the massive star WR104," *Nature* **398**, pp. 487–489, Apr. 1999.

[19] R. Soummer, A. Sivaramakrishnan, B. R. Oppenheimer, R. Roberts, D. Brenner, A. Carlotti, L. Pueyo, B. Macintosh, B. Bauman, L. Saddlemyer, D. Palmer, D. Erickson, C. Dorrer, K. Caputa, C. Marois, K. Wallace, E. Griffiths, and J. Mey, "The Gemini Planet Imager coronagraph testbed," in *Society of Photo-Optical Instrumentation Engineers (SPIE) Conference Series*, *Society of Photo-Optical Instrumentation Engineers (SPIE) Conference Series* **7440**, Aug. 2009.